New Phytologist

Research

In vivo visualization of the final stages of xylem vessel refilling in grapevine (*Vitis vinifera*) stems

Craig R. Brodersen[1], Thorsten Knipfer[2] and Andrew J. McElrone[2,3]

[1]School of Forestry and Environmental Studies, Yale University, New Haven, CT 06511, USA; [2]Department of Viticulture and Enology, University of California, Davis, CA 95618, USA; [3]Crops Pathology and Genetics Research Unit, USDA-ARS, Davis, CA 95618, USA

Author for correspondence:
Craig R. Brodersen
Tel: +1 203 436 5145
Email: craig.brodersen@yale.edu

Received: *23 June 2017*
Accepted: *22 August 2017*

New Phytologist (2017)
doi: 10.1111/nph.14811

Key words: cavitation, embolism, grapevine, refilling, *Vitis vinifera*, X-ray micro-computed tomography (microCT), xylem.

Summary

- Embolism removal is critical for restoring hydraulic pathways in some plants, as residual gas bubbles should expand when vessels are reconnected to the transpiration stream. Much of our understanding of embolism removal remains theoretical as a consequence of the lack of *in vivo* images of the process at high magnification.
- Here, we used *in vivo* X-ray micro-computed tomography (microCT) to visualize the final stages of xylem refilling in grapevine (*Vitis vinifera*) paired with scanning electron microscopy.
- Before refilling, vessel walls were covered with a surface film, but vessel perforation plate openings and intervessel pits were filled with air. Bubbles were removed from intervessel pits first, followed by bubbles within perforation plates, which hold the last volumes of air which eventually dissolve. Perforation plates were dimorphic, with more steeply angled scalariform plates in narrow diameter vessels, compared with the simple perforation plates in older secondary xylem, which may favor rapid refilling and compartmentalization of embolisms that occur in small vessels, while promoting high hydraulic conductivity in large vessels.
- Our study provides direct visual evidence of the spatial and temporal dynamics of the final stages of embolism removal.

Introduction

The cohesion–tension theory of water transport in plants is the guiding framework for our understanding of how water moves through vascular plants from the soil to the atmosphere. Two core principles of this theory are: (1) xylem sap is transported under negative pressure, and (2) conduits and xylem sap must necessarily be free of any large gas bubbles which would rapidly expand under the negative pressure environment stipulated in (1), although the xylem sap can be saturated with dissolved gasses (e.g. Scholander *et al.*, 1955; Schenk *et al.*, 2017). Numerous studies measuring losses in hydraulic conductivity in addition to direct, *in vivo* visualizations of xylem during drought (e.g. Brodersen *et al.*, 2013; Choat *et al.*, 2015) have shown that gas embolisms form in the xylem conduits, leading to significant declines in hydraulic conductivity (Brodribb & Cochard, 2009; Choat *et al.*, 2012; Urli *et al.*, 2013).

Evidence of embolism removal has been documented for over 30 yr (Sperry *et al.*, 1987) and various imaging techniques have played a critical role in describing the phenomenon in an effort to better understand the underlying mechanism by which gas bubbles are replaced with water (Canny, 1997; Tyree *et al.*, 1999; Holbrook *et al.*, 2001; Brodersen *et al.*, 2010; Knipfer *et al.*, 2015b, 2016; Rolland *et al.*, 2015). Embolism removal can apparently be accomplished by nonmutually exclusive mechanisms (Brodersen *et al.*, 2013). Gas bubbles in the xylem conduits of some species can dissolve on their own (Lee & Kim, 2008; Rolland *et al.*, 2015; Ryu *et al.*, 2016), a process which is governed by temperature, the surface tension of water, plant water potential (Ψ_{stem}), conduit diameter, and wall surface properties (e.g. hydrophobicity and wall sculpturing; Konrad & Roth-Nebelsick, 2005; Kohonen & Helland, 2009; Rolland *et al.*, 2015). This mechanism involves the dissolution of gas bubbles into the surrounding xylem sap at the gas−water interface. A second mechanism has been proposed which involves an influx of water into embolized vessels from the surrounding living cells in the xylem (e.g. parenchyma and fibers), and has been observed in both intact (Canny, 1997; Tyree *et al.*, 1999; Brodersen *et al.*, 2010) and excised stems (Knipfer *et al.*, 2016). Observations from the Knipfer *et al.* (2016) study suggest that, while positive pressure generated by roots can indirectly facilitate the embolism removal process, connectivity to the root system is not required, probably because of morphological and functional similarity in the generation of positive pressure in root and stem xylem (see Wegner, 2013). During this process, water droplets grow at predictable rates and coalesce, and the trapped gas bubbles decrease in volume and eventually collapse, with the gas presumably diffusing into the surrounding solution (Brodersen *et al.*, 2010; Knipfer *et al.*, 2015b). This phenomenon has been documented in several grapevine species, and is possibly at work in other

species (Brodersen & McElrone, 2013), although refilling is by no means a universal trait in woody plants (Choat *et al.*, 2015; Knipfer *et al.*, 2015a,b).

Recent experiments have provided evidence for an additional, complementary mechanism for gas removal or stabilization of bubbles in the xylem sap, whereby large bubbles trapped in intervessel pits are reduced to *c.* 50–250 nm radius (radii measured at atmospheric pressure), the stability of which is achieved through surfactant coatings acquired during their passage through the pit membrane (Schenk *et al.*, 2015, 2017). The coatings prevent nanobubbles from growing to a critical threshold radius that would otherwise cause them to expand (Oertli, 1971; Schenk *et al.*, 2015, 2017). While some clarity has been achieved at the nano-scale, and through *in vivo* observations at the whole stem and vessel levels, uncertainty still remains around the fate of residual gas bubbles during the final stages of embolism repair before the nanobubble phase.

The current theoretical framework posits that pit chambers should hold the last remaining volumes of gas (Holbrook & Zwieniecki, 1999; Clearwater & Goldstein, 2005). Without the removal of residual gas bubbles greater than a critical radius (Oertli, 1971; Yang & Tyree, 1992) the vessel should be at risk of subsequent hydraulic failure as soon as the xylem sap reaches sustained negative pressures and is reconnected to the transpiration stream. A second hypothesized location where gas bubbles could become trapped are the openings of perforation plates that separate vessel elements, in particular those of the scalariform type (Tyree & Zimmermann, 2002). However, the presence of gas in those perforations would lead to the same problem as residual gas trapped in the intervessel pits. How and when the last remaining volumes of gas are removed have remained unresolved largely as a consequence of the difficulty in visualizing this process *in vivo*. Previous efforts at visualizing the functional status of the xylem network with nondestructive imaging tools (Holbrook *et al.*, 2001; Brodersen *et al.*, 2010; Cochard *et al.*, 2015) have largely fallen short of documenting the dynamics of embolism removal within the microstructures that trap gas bubbles in the vessel walls as a consequence of insufficient spatial and temporal resolution of existing imaging systems. Here, we used time-lapse high-resolution X-ray micro-tomography (microCT) imaging with a spatial resolution of 650 nm^3 to visualize the final stages of embolism removal in grapevine (*Vitis vinifera* 'Thompson Seedless').

Materials and Methods

To visualize the functional status of grapevine (*Vitis vinifera* L. cv 'Thompson Seedless') vessels *in vivo*, and specifically the anatomical components where gas could remain trapped, we used time-lapse high-resolution X-ray micro-computed tomography (microCT) imaging at the Lawrence Berkeley National Laboratory, Beamline 8.3.2 (Berkeley, CA, USA). Grapevines were grown in a glasshouse from cuttings in 10 × 10 × 10 cm, 0.7-l plastic pots (#AB45; Stuewe and Sons, Tangent, OR, USA) filled with montmorillonite fritted clay (Turface MVP; Profile Products, Buffalo Grove, IL, USA), irrigated daily and fertilized weekly with half-strength Hoagland's solution. Plants were grown to a height of 50 cm with 10–15 leaves, and had a single stem diameter of < 8 mm at 10 cm above the soil surface. The plants were *c.* 9–12 months old at the time of the experiment. The potted plants were transported by car from the University of California (UC) Davis glasshouse to Beamline 8.3.2 on the day of the scans. An initial bagged leaf water potential value was measured upon arrival at the facility (#3000; Soil Moisture Equipment, Golita, CA, USA), with this equilibrated value used as an estimate of the water potential of the stem. Periodic water potential measurements were taken as the plants dried to *c.* −1.0 MPa, a value known to induce mild drought stress and some embolism in the xylem (Brodersen *et al.*, 2010, 2013) but still hydrated enough to allow the initiation of refilling within 60–90 min after the soil was saturated (Supporting Information Fig. S1). Stem psychrometers were not used because the stem diameters were below the minimum thickness necessary for creating a vapor seal. Once the four plants had reached a stem water potential of *c.* −1.0 MPa they were mounted in a custom potholder on the sample stage, and enclosed in an acrylic cylinder to minimize plant movement during the scan. Stems were then scanned 10 cm above the soil surface at 24 keV in continuous tomography mode, producing 1025 two-dimensional projection images as the plant rotated 180° in the X-ray source. The projection images were then reconstructed using Octopus 8.6 (Institute for Nuclear Sciences, Ghent University, Ghent, Belgium) and visualized with the Avizo 8 software package (FEI, Houston, TX, USA). The initial scans were first captured at low magnification (×2 lens) to view the entire cross-section of the stem and identify a region of interest for investigations at higher magnification (Fig. 1). Using the ×10 lens to visualize refilling in a small section of the xylem produced an effective voxel (volumetric pixel element) size of 0.65 μm^3 for our images. At the ×10 magnification it was possible to visualize only a subvolume of the entire stem *c.* 4 mm^3 (1.7 × 1.7 × 1.4 mm; Fig. 1b). After the initial scan, the plants were watered to field capacity. The plants were then rescanned *c.* every 60 min for up to 8 h (Fig. S1). We did not observe any visual evidence of X-ray damage resulting from repeated scans. After the last scan, a final bagged leaf water potential measurement was taken to determine the water status of the stem. Plants inside the microCT hutch were in a dark environment, and periodic porometer measurements (#SC-1; Decagon, Pullman, WA, USA) were taken to determine whether the plants were transpiring.

Our microCT images showed the presence of steeply inclined scalariform perforation plates within the xylem (Frost, 1930), predominantly in the small diameter primary xylem vessels near the pith. We also observed unusual simple perforation plates intergraded with pit-like perforations at the plate margins (Meylan & Butterfield, 1975; Carlquist, 2001; Fig. 2). To characterize these perforation plates and their distribution within the scanned tissue, we measured the plate contact angle and length, the vessel diameter, and distance from the nearest pith cell (used as a spatial reference point) of all perforation plates visible in four different plants within the field of view. The perforation plate contact angle was defined as the acute angle at which the plate extended from the vessel wall. These measurements were performed with the measurement tool in Avizo 8.0. Statistical analyses, graphing,

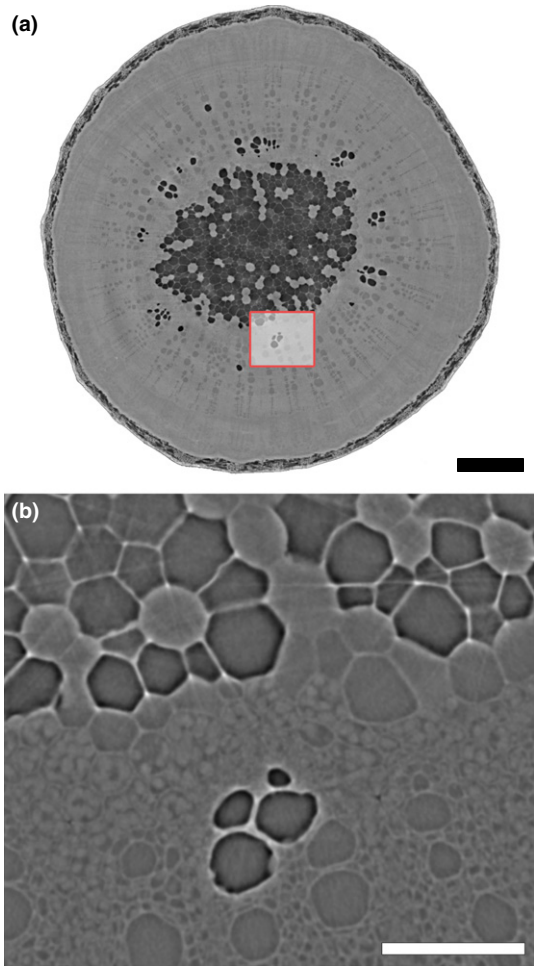

Fig. 1 *In vivo* transverse X-ray micro-computed tomography (microCT) cross-sections of a *Vitis vinifera* stem at (a) low and (b) high magnification to illustrate the tradeoff between field of view and spatial resolution. The area within the red box in (a) is shown at higher magnification in (b). Dark regions within the images are air-filled, while the gray areas are water-filled tissue. In (b) a vessel group is shown in the early stages of refilling. Bars: (a) 500 μm; (b) 125 μm.

and curve fitting were performed in SigmaPlot (Systat Software Inc., San Jose, CA, USA) and R (R Core Team, 2013) with the Ggplot2 package (http://ggplot2.org). We also measured the liquid wall contact angle for 55 vessels using the angle measurement tool in Avizo on images that bisected the droplet longitudinally.

Fresh stem internodes from plants growing in similar glasshouse conditions and of similar developmental age were shipped overnight from UC Davis to Yale University (New Haven, CT, USA) for imaging with an environmental scanning electron microscope (ESEM; XL30 FEI/Philips, Houston, TX, USA) at 10 kV operated under true Environmental mode. This analysis was performed to characterize the microstructure of the sites where small bubbles were observed to accumulate in the microCT images. The resolution of the microCT images was insufficient to determine the presence of structures such as pit membranes. The samples were dissected with a razor blade to expose longitudinal sections of the xylem. The exposed sample faces were *c.* 3 mm^2 and were mounted on a Peltier cooled stage (FEI/Philips) maintained at 0.5°C. Water vapor was injected into the sample chamber at 4.0 Torr water vapor pressure, thereby establishing 95% relative humidity, to prevent desiccation. With this sample preparation, no sputter coating was required. Perforation plates and intervessel pits were located within the sample and the presence of pit membranes was visually confirmed. To determine the presence of pit membranes in the scalariform pitting that was often found adjacent to the large simple perforations in the angled vessel element perforations of large-diameter vessels, regions where the pit border (secondary cell wall) had been broken during the dissection process were visualized (e.g. Fig. 2c).

Results

Stem water potential values recovered quickly after soil saturation, similar to values reported for this species in previous studies (Holbrook *et al.*, 2001; Brodersen *et al.*, 2010; Knipfer *et al.*, 2015b, 2016). Before watering, bagged leaf water potentials ranged from −1.3 to −1.7 MPa, and recovered to −0.3 to −0.5 MPa within 2–3 h and then remained stable (Fig. S1). Throughout the experiment, stomatal conductance measurements were all < 20 mmol m^{-2} s^{-1} (i.e. negligible and predominantly cuticular).

Using higher magnification imaging compared with our previous studies decreased the field of view, but significantly improved the spatial resolution necessary to resolve localized fine-scale refilling processes within the microstructures that trap gas bubbles in the vessel walls (Brodersen *et al.*, 2010; Knipfer *et al.*, 2015b; Fig. 1).

Before refilling, the intervessel pits were air-filled, but a surface film was present and obscured the vessel-parenchyma pitting that should have been visible given the dimensions of the pits observed with the ESEM (Fig. 3). Water droplets then emerged from the vessel-parenchyma pits, and proceeded to cover pit-like openings adjacent to the large simple perforations, but those openings did not immediately fill (Figs 2a, 4). Mean droplet contact angle was 59.58° ± 12.18° SD, with a minimum and maximum contact angle of 24.5° and 80.3°, respectively ($n = 55$). Water droplets with a contact angle > 90° were rare, but we did observe some cases where the contact angle was different on opposite sides of the droplet, similar to Brodersen *et al.* (2010) and Knipfer *et al.* (2015b). Even after the lumen filled, some bubbles remained trapped in these openings (Fig. 4c, gray arrowhead). As the vessel lumen filled with water, the intervessel pits refilled (Fig. 5), but with a time delay after coming into contact with the emerging droplets which spread over the vessel walls. Internal surfaces of the bordered pits appeared to be hydrophobic, holding small volumes of gas even when water droplets covered their openings or when the vessel lumen was filled with water (Fig. 4c, white arrowhead). Next, bubbles were compressed into progressively smaller volumes, and were often pushed up against the scalariform perforation plates in small-diameter vessels and eventually dissolved (Fig. 6).

When consecutive gas-filled vessel elements were separated by scalariform perforation plates, the perforation appeared to

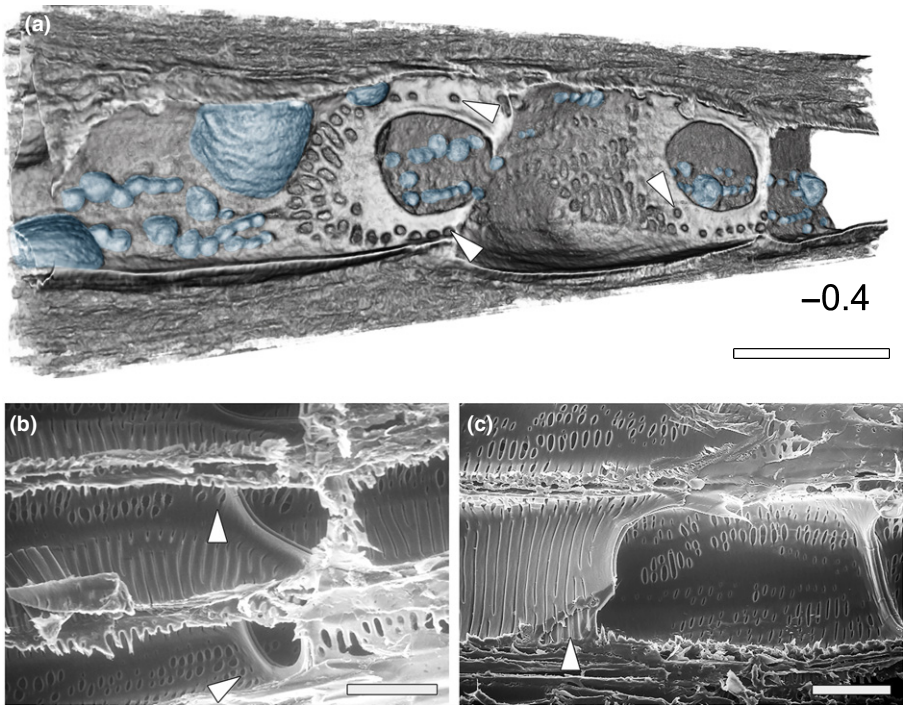

Fig. 2 *Vitis vinifera* vessels exposed longitudinally and imaged using *in vivo* X-ray micro-computed tomography (microCT) (a) and environmental scanning electron microscopy (ESEM; b, c) allow for detailed observation of the xylem microstructure related to embolism removal. The *in vivo* microCT image (a) shows the spatial heterogeneity of water droplet growth from the vessel-parenchyma pitting (droplets are false colored in blue). Simple perforations between vessel elements were often intergraded with multi-perforate regions (white arrowheads in a, b) which did not contain pit membranes (c, white arrowhead). Bars: (a) 100 μm; (b) 20 μm; (c) 50 μm. Stem water potential value is noted in (a).

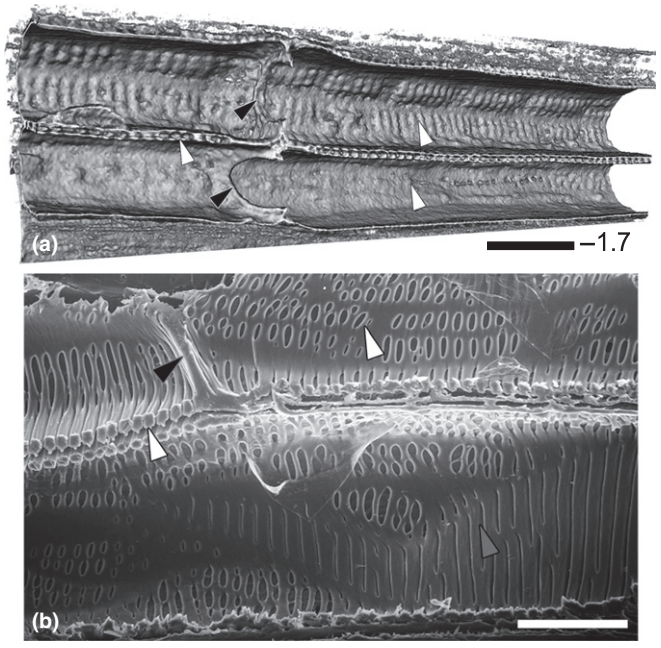

Fig. 3 Longitudinal views of *Vitis vinifera* xylem vessels with (a) X-ray micro-computed tomography (microCT) and (b) environmental scanning electron microscopy (ESEM). The two imaging methods show the difference between recently embolized tissue (a), where a surface film of water adheres to the vessel walls (white arrowheads) covering the intervessel, and vessel-parenchyma pitting. The intervessel pitting (white arrowhead, left side) is air-filled. With ESEM imaging, the surface film has evaporated, revealing the pitting. Simple perforations are not obscured in either method (black arrowheads). Bars, 50 μm. Stem water potential is noted in (a).

be completely gas-filled before soil saturation (Figs 6, 7). Longitudinal microCT sections showed that, when one of the two adjacent vessel elements separated by a scalariform perforation plate was filled with water, the openings remained gas-filled (Figs 6d, 7e). Water advanced up to the perforation plate openings, but did not fill them (Figs 6d, 7a,e). For example, in Fig. 7(f), 57 min after soil saturation the lower vessel element filled with water but gas remained in all six of the visible perforation plate openings. Approximately 60 min later, gas in four of the six visible perforations plate openings was replaced with water (Fig. 7c,g). Over the next 300 min, the remaining two empty perforations filled with water (Fig. 7d,h) while the functional status of the vessel remained stable (i.e. it did not embolize). In all cases, gas trapped in the perforation plate openings persisted for hours (Figs 6, 7). In one case, adjacent perforation plate openings filled sequentially (Fig. 7f–h), starting close to one vessel wall and then progressing across the perforation plate to the opposite wall.

Stem scans made before soil saturation when many of the vessels were filled with gas allowed us to visualize the differences in vessel anatomy in those regions of interest, including the distribution and morphology of the perforation plates. We observed a strong dimorphism in perforation plates across the primary and secondary xylem. Most vessel element perforations were simple, and nearly transverse, where the aperture was nearly the full width of the vessel (Figs 3a, black arrowhead; 4a, white arrowhead). However, we identified 152 angled perforation plates that were characterized as either (1) bordered simple perforation plates intergraded with pit-like perforations at their margins ($n = 87$) (Fig. 2a, white arrowhead), where the aperture of the simple perforations constricted to *c.* 1/3 to 1/2 the diameter of the vessel; or (2) scalariform perforation plates ($n = 65$; Fig. 8). Scalariform perforation plates were found almost exclusively within vessels smaller than 45 μm in diameter, and often in primary xylem with helical thickenings. Angled simple perforation plates were typically found in larger diameter vessels (Fig. 8).

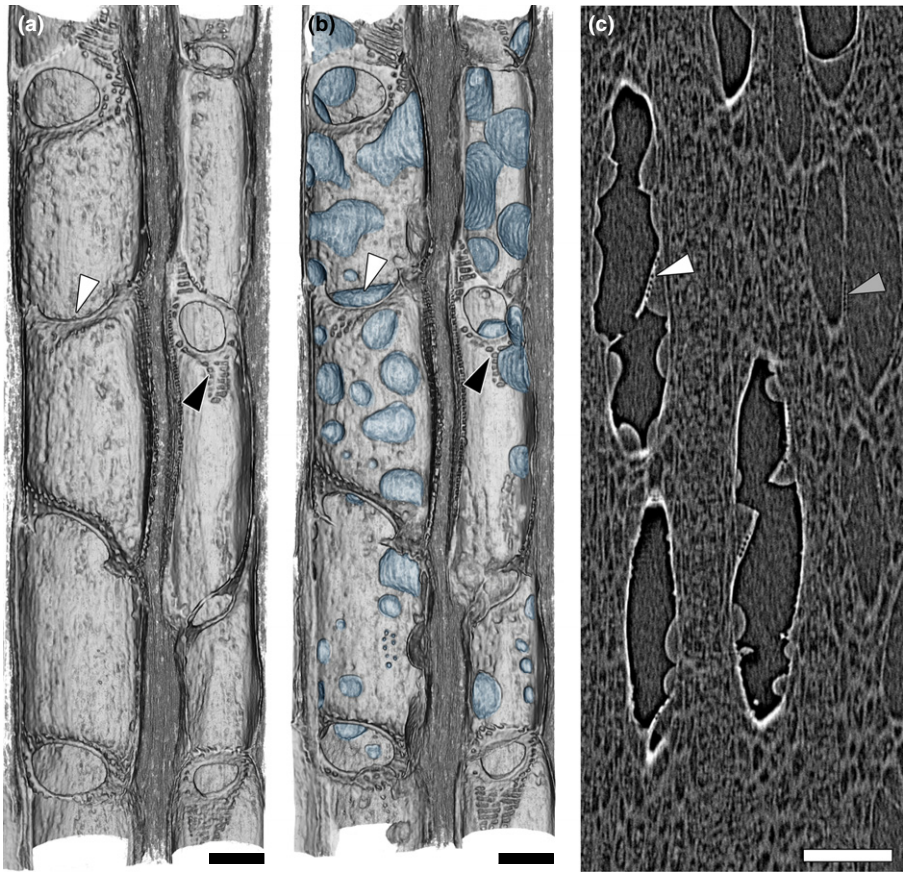

Fig. 4 Longitudinal *in vivo* X-ray micro-computed tomography (microCT) images through two neighboring *Vitis vinifera* vessels taken *c.* 4 h apart. Before refilling (a; −1.6 MPa) much of the vessel walls is covered with a surface film of water, while openings in the angled perforation plates are air-filled (black arrowheads). During the droplet growth phase (b), water droplets emerge from the vessel walls adjacent to xylem parenchyma or fibers on the opposite side of the vessel wall (droplets are false colored in blue). Water accumulates where angled perforation plates extend from the vessel wall (white arrowheads in a and b), and grow over the small pit-like perforations adjacent to the large, simple perforation (black arrowheads in a, b; white arrowhead in c). An oblique two-dimensional cross-section (c) bisects the vessels shown in (a) and (b), and also bisects a water-filled vessel where the pit-like perforations in the perforation plate have not filled with water (gray arrowhead in c). Bars: (a, b) 50 μm; (c) 100 μm. Stem water potential was −1.6, −0.4, and −0.4 MPa, in (a), (b) and (c), respectively.

There was a significant linear relationship between vessel diameter and scalariform perforation plate angle at which it intersected the vessel wall ($r^2 = 0.42$; $P < 0.001$), but no relationship in vessels with simple perforation plates ($r^2 = 0.07$; $P = 0.014$; Fig. 8b). There was also a significant relationship between the perforation plate angle and the length of the plate ($r^2 = 0.51$; $P < 0.0001$; Fig. 8c) that was best fitted with a hyperbolic decay function (i.e. longer perforation plates had steeper angles).

The microCT images did not resolve the presence or absence of pit membranes in the intervessel walls. MicroCT images showed that, when the vessel lumens were filled with gas, both intervessel pits and the scalariform perforations were also gas-filled (Figs 6, 7). The stability of the bubbles within the steeply angled scalariform perforation plates of small-diameter vessels led to some uncertainty about whether pit membranes were present. ESEM imaging of equivalent structures within the xylem of additional plants (i.e. these were not scanned with microCT) revealed that pit membranes were present in intervessel pits (Fig. 3), but absent in the scalariform and pit-like perforations adjacent to the simple perforations (Fig. 2c). ESEM images suggest that pit membrane remnants were present in the scalariform perforation plates we observed in small-diameter vessels (Fig. 9).

Discussion

These *in vivo*, high-resolution time-lapse microCT images of embolism removal in grapevine offer a new view of the final stages of a biophysical process that plays a critical role in drought recovery of grapevine and, potentially, other species (Brodersen & McElrone, 2013). Notably, these images provide visual confirmation that lateral intervessel connections and perforation plates are the loci for trapped gas bubbles in a refilling vessel, but also raise additional questions about the exact mechanisms at play.

Gas bubbles were present in intervessel pits and perforation plates when the vessels were fully embolized, and these bubbles remained stable in perforation plate openings for up to 8 h in one case (Figs 6, 7), suggesting that (1) the xylem sap pressure in the refilling vessel lumen was such that it prevented water from flooding into these spaces, and/or (2) the internal surfaces of the pit and perforation borders are sufficiently hydrophobic to overcome the advance of water across the aperture (Figs 4–7). Variable droplet contact angles (typically < 90°) and the hydrophobic pit chambers strongly suggest spatial heterogeneity in vessel wall surface properties (McCully *et al.*, 2014). The mean water droplet contact angle was 59.6°, which was lower than values reported for *Vitis riparia* (64°; Knipfer *et al.*, 2016) and *V. vinifera* cv 'Chardonnay' (94°, but both hydrophobic and hydrophyllic surfaces were reported; Brodersen *et al.*, 2010). These data suggest that, within a genus and species, there can be considerable variability in vessel wall surface properties, which has been shown in other species (McCully *et al.*, 2014). It is also worth noting that our images of droplets on the vessel walls bear a striking resemblance to those imaged in *Laurus nobilis* vessels with cryo-SEM by Tyree *et al.* (1999).

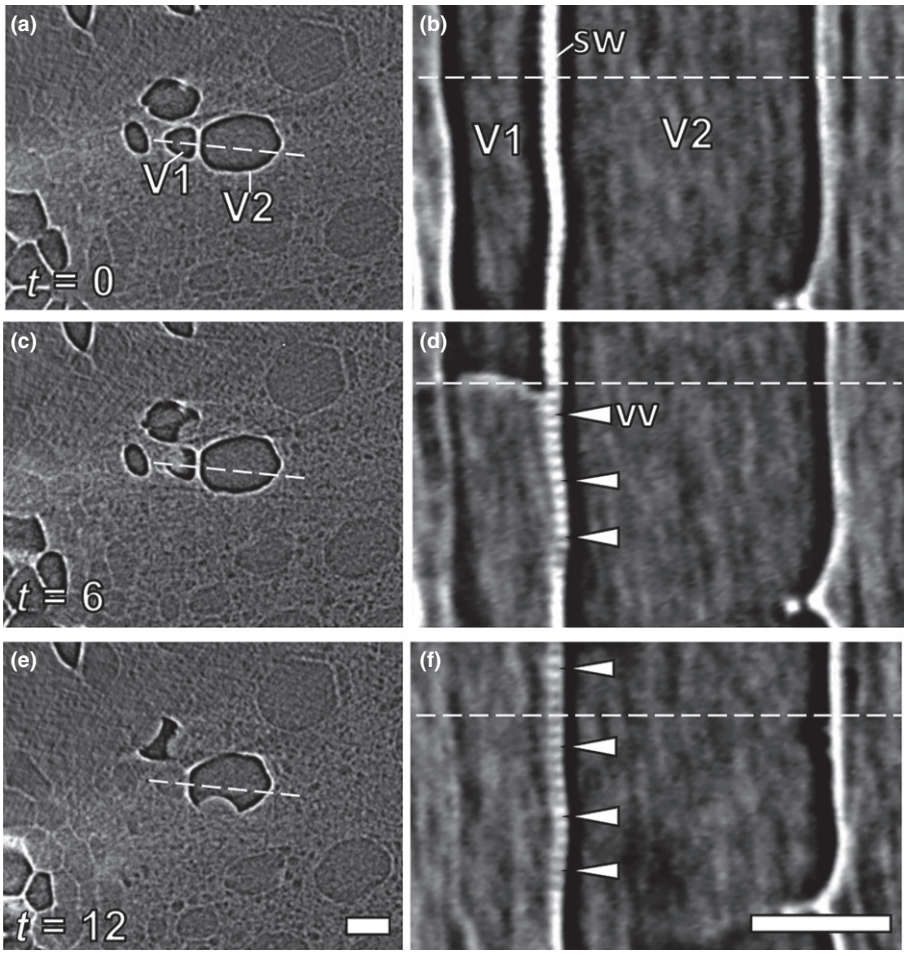

Fig. 5 Representative X-ray micro-computed tomography (microCT) time series of refilling in the intervessel walls of *Vitis vinifera*. Transverse cross-sections (a, c, e) with corresponding longitudinal sections of the same vessels (b, d, f) are shown. Dashed lines in (a), (c) and (e) indicate the position of paired longitudinal images in (b), (d) and (f). At time $t = 0$ h, the vessel lumen of both vessels V1 and V2 was air-filled (dark gray color). At $t = 6$ h, a water column had grown from individual droplets to expand and intervessel pitting had filled with water. At $t = 12$ h, more intervessel pits refilled (f). vv, intervessel pitting; sw, side (lateral) wall. Bars, 50 μm.

The surface film of water that was present on the vessel walls and obscured the vessel-parenchyma pits suggests that when a vessel embolizes most, but not all, of the water is removed (Figs 2, 3). This film, however, does not cover all of the surfaces, including the perforation plates that extend from the vessel wall (Figs 2, 4). This observation along with the nonzero contact angles of water droplets appressed to the perforation plates suggests that these surfaces, along with other portions of the vessel wall, are hydrophobic. The pressure of the xylem sap at this interface is probably the net effect of the growing water droplets from the refilling process counteracted by the water in the surrounding vessels and living tissue. Holbrook & Zwieniecki (1999) suggested that gas trapped in these small spaces would dissolve across this gas–water interface and the bubbles would be slowly removed. However, for this mechanism to work over a short time period, water would need to be flowing in neighboring vessels to establish a diffusion gradient that would carry away the gas-saturated water, which was probably not happening in our plants which showed negligible transpiration rates. Furthermore, the hydrostatic connection to functional vessels transporting water would come with the significant risk of water in the refilling vessel being pulled into the transpiration stream leading to refilling failures, as demonstrated previously (Brodersen *et al.*, 2010). Our images instead suggest that the intervessel pits fill during the droplet growth stage (Fig. 5), followed by the dissolution of bubbles at the perforation plates (Figs 6, 7). Bubbles persisting in the perforation plate openings after the lumen had filled were stable for hours, as predicted by Konrad & Roth-Nebelsick (2005) for bubbles of this size, but eventually dissolved.

The observed −0.6 MPa Ψ_{stem} recovery threshold required for refilling in this species (Brodersen *et al.*, 2010; Knipfer *et al.*, 2015b, 2016) presents a number of theoretical challenges to our understanding of refilling. The first is that it remains to be shown experimentally if the equilibrated water potential measured on bagged leaves using a Scholander pressure chamber is representative of xylem pressure, and if some heterogeneity of water potentials and hydrostatic isolation must exist within the refilling tissue (i.e. positive pressure in some isolated locations, and negative in others). If not, any residual large bubbles larger than the critical bubble radius would expand and refilling would fail (Oertli, 1971).

Given the resolution limitations of our imaging system, we could not find visual evidence of nanobubbles (Schenk *et al.*, 2017), but all visible bubbles were above the critical radius i.e. unstable at the measured water potentials. Thus, the bulk Ψ_{stem} values estimated from bagged, equilibrated leaves *c.* 10–15 cm from the scanned area may not be of sufficient resolution and accuracy to correspond directly to localized xylem pressure of the

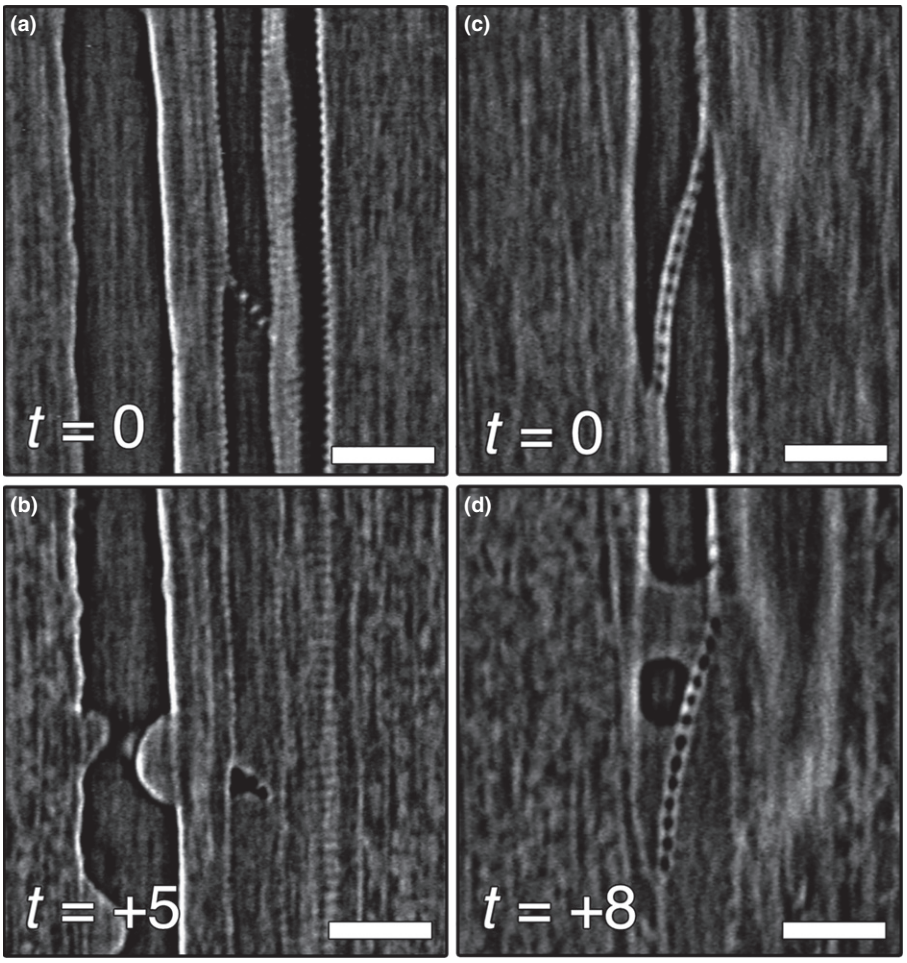

Fig. 6 Representative refilling heterogeneity in two pairs of adjacent *Vitis vinifera* vessel elements separated by a scalariform perforation plate before (a, c) and after (b, d) soil saturation. In the first vessel pair (a, b), scalariform perforations were air-filled when the vessel was embolized, and retained the last volumes of air as the advancing meniscus approached the perforation plate. In the second vessel pair (c, d), the perforation plate openings are clearly air-filled (black circular regions in the angled perforation plate), and bubbles of various size accumulate at this barrier, and eventually dissolve. Bars, 50 μm. Stem water potentials were −1.6 MPa in (a) and (c), and −0.4 and −0.3 MPa in (b) and (d), respectively. Time of each scan is noted in hours.

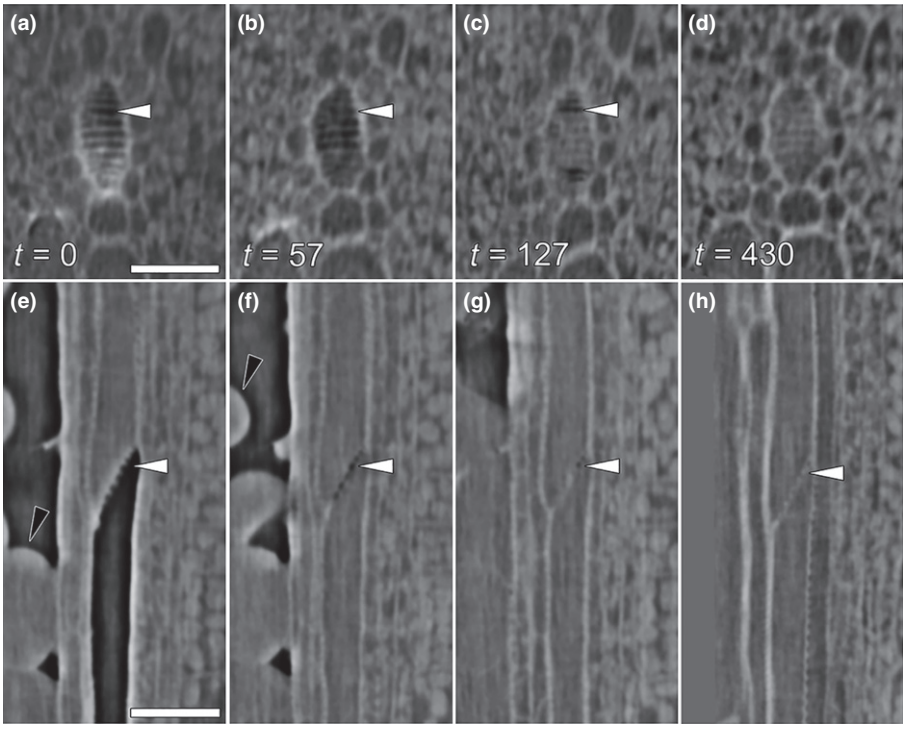

Fig. 7 Progression of refilling in a *Vitis vinifera* scalariform perforation plate over 430 min observed in paired oblique (a–d) and longitudinal (e–h) micro-computed tomography (microCT) sections. Water droplet growth typical of grapevine was visible (black arrowheads in e and f). Scalariform perforations begin gas-filled and then fill sequentially (white arrowheads). Time stamps in (a–d) are in minutes from the time of the initial scan ($t = 0$). Equilibrated stem water potentials were −0.4 and −0.3 MPa at $t = 0$ and $t = 430$, respectively. Bars, 50 μm for all panels.

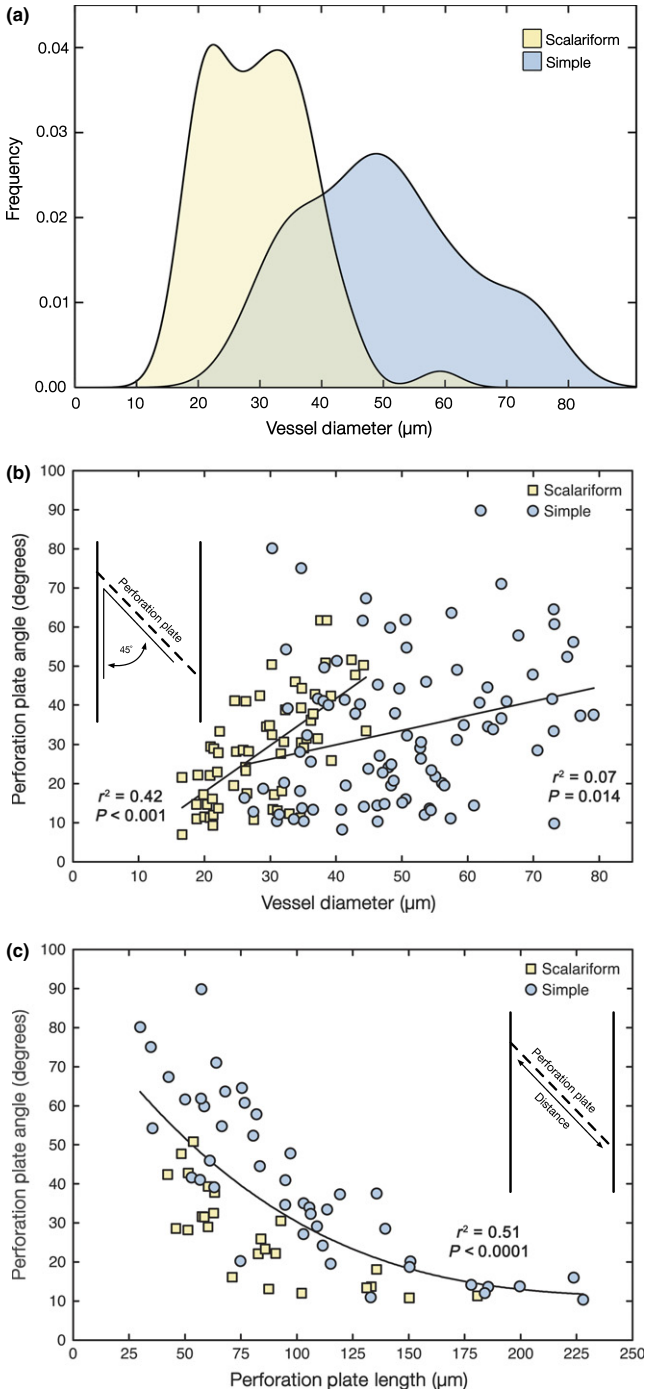

Fig. 8 Characterization of the perforation plates in *Vitis vinifera* xylem. (a) Density distribution of scalariform (yellow, $n = 65$) and simple (blue, $n = 87$) angled perforation plates located within 500 μm of the pith. The relationship is shown between perforation plate contact angle relative to the vessel wall and (b) vessel diameter and (c) perforation plate length in scalariform (yellow squares) and simple (blue circles) perforation plates. Insets in (b) and (c) indicate how the angle and length were defined and measured. Linear regression (b) and (hyperbolic) curves are fitted to the data, with r^2 and P values inset in each panel.

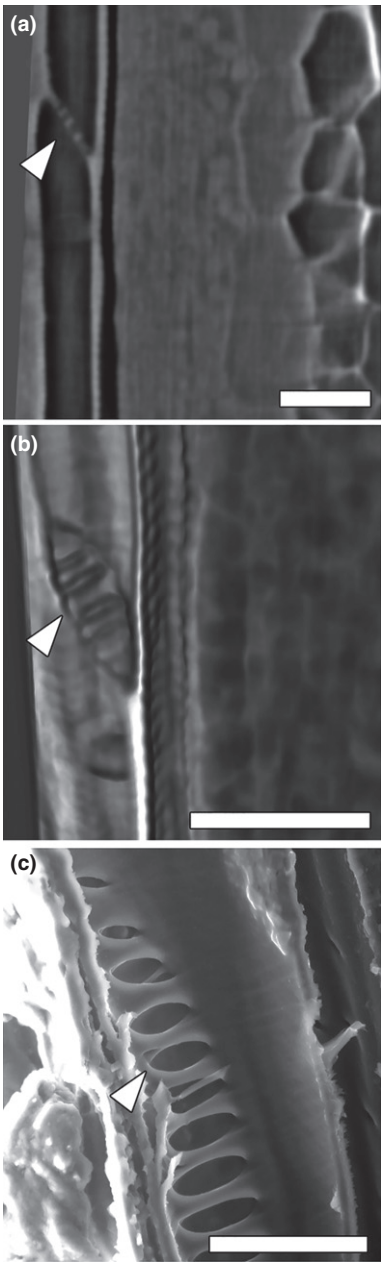

Fig. 9 Steeply angled *Vitis vinifera* scalariform perforation plates were visible in (a) two-dimensional and (b) three-dimensional X-ray micro-computed tomography (microCT) images. These perforation plates were the locus of the final volumes of gas in the refilling vessels, but microCT could not resolve the internal structure. In (c), environmental scanning electron microscopy (ESEM) was used to visualize the scalariform perforation plates, and pit membranes were present. It is unclear whether the pit membranes were completely intact. White arrowheads point to scalariform bars in each panel. Bars: (a, b) 50 μm; (c) 20 μm.

actively refilling tissue. Once the −0.6 MPa Ψ_{stem} is achieved after soil saturation, that negative pressure would still exceed the capillary pressure threshold of the perforation plate openings by order of magnitude (estimated at −0.06 MPa capillary pressure using the method of Cochard *et al.*, 2009). All plants in this study recovered to −0.3 to −0.4 MPa during our experiments, but those negative pressures still exceed the calculated threshold, yet the vessels refilled. Grapevine stem xylem appears to be hydraulically segmented, both between different tissue types in the plant (Hochberg *et al.*, 2017) and within explicit functional domains

of the stem (Brodersen *et al.*, 2011), with discrete groups of vessels providing long-distance axial water transport, while other zones supply water to leaves, tendrils, and fruit. Our visualizations were limited to the dorsal/ventral zones which may be hydraulically isolated from the lateral zones connected to the leaves that were used for Ψ_{stem} measurements. Thus, knowing the actual water potential of tissues at this scale is difficult, and recent evidence suggests that water potential gradients within the plant can apparently preclude refilling at tissues far from the root–soil interface (Charrier *et al.*, 2016).

When embolisms arise in grapevine xylem they tend to completely fill vessels (Brodersen *et al.*, 2010, 2013; Knipfer *et al.*, 2015b, 2016). Thus, the refilling mechanism must remove large volumes of gas from the xylem, particularly in the older large-diameter vessels. Indeed, our previous work (Brodersen *et al.*, 2010; Knipfer *et al.*, 2015b) has shown that small-diameter vessels near the pith filled more quickly than large-diameter vessels farther from the pith. However, this may not be attributable entirely to conduit diameter, and the dimorphic perforation plates and their distribution observed in our refilling plants provide some additional insight. Our observations showing that the last gas bubbles are located within the scalariform perforation plates (Figs 6, 7) suggest that the observed radial heterogeneity in the distribution of simple and scalariform perforation plates could be physiologically relevant. More frequent scalariform perforation plates could lead to many smaller bubbles rather than one large bubble that would form in a vessel with only simple perforations, leading to a more favorable surface area to volume ratio for faster dissolution of gas (Ewers, 1985; Sperry, 1985; Tyree & Zimmermann, 2002). However, the scalariform bars would also impose added resistance to water transport, which may help to explain why scalariform perforation plates were found less frequently in the large-diameter xylem vessels farther from the pith (Fig. 8). Christman & Sperry (2010) found that in woody plants a decrease in scalariform perforation plate angle (i.e. a steeper plate) led to greater hydraulic resistance, which was attributed to greater surface area of the scalariform bars and therefore increased frictional resistance to water. Here, we found that perforation plate angle increased with increasing vessel diameter and developmental age (Fig. 8b). While it is unclear what fraction of the scalariform perforation plates contain pit membrane remnants (Fig. 9), their resistance combined with that of the scalariform bars would significantly reduce the hydraulic efficiency of these vessels.

While scalariform perforation plates are thought to be the ancestral state, it is clear that they have been retained in numerous species from both tropical and temperate habitats (Frost, 1930; Baas & Wheeler, 1996; Sperry, 2003; Lens *et al.*, 2016), including grapevine, although selectively in the young, primary xylem (Fig. 8). A mixture of simple and scalariform perforation plates can be found in other genera (Bierhorst & Zamora, 1965; Meylan & Butterfield, 1975; Butterfield *et al.*, 1984; Oskolski & Jansen, 2009), and scalariform perforation plates can be more common in narrow vessels (Carlquist, 2001). Tyree & Zimmermann (2002) and Sperry (1985) also suggested that the scalariform bars could function in trapping bubbles following freeze–thaw events, but others have shown that simple perforation plates can accomplish the same task (Ewers, 1985; Davis *et al.*, 1999; Rolland *et al.*, 2015).

Conclusions

Our data provide a rare glimpse into the spatial and temporal complexity of the embolism repair mechanism in grapevine, and provide a new platform for studying this enigmatic process. Clearly, more work is needed in determining the both the heterogeneity in vessel wall and perforation plate hydrophobicity, as well as the influence of the surface film on the droplet growth phase of refilling. Additional insight into these details, as well as the true water potential of the surrounding tissue, will be important components to a more robust explanation for how refilling is accomplished.

Acknowledgements

The authors kindly thank D. Parkinson and A. MacDowell for their assistance at the Lawrence Berkeley National Laboratory Advanced Light Source Beamline 8.3.2 microtomography facility. The Advanced Light Source is supported by the Director, Office of Science, Office of Basic Energy Services, of the US Department of Energy under contract no. DE-AC01-05CH11231. This research was funded in part by the USDA-ARS Sustainable Viticulture Production Systems CRIS Project 2032-21220-006-00, NP305 Crop Production.

Author contributions

C.R.B., T.K. and A.J.M. planned, designed, and performed the research. C.R.B. and T.K. analyzed the data. C.R.B., T.K. and A.J.M. wrote the manuscript.

References

Baas P, Wheeler EA. 1996. Parallelism and reversibility in xylem evolution a review. *IAWA Journal* **17**: 351–364.

Bierhorst DW, Zamora PM. 1965. Primary xylem elements and element associations of angiosperms. *American Journal of Botany* **52**: 657–710.

Brodersen C, McElrone A. 2013. Maintenance of xylem network transport capacity: a review of embolism repair in vascular plants. *Frontiers in Plant Science* **4**: 108.

Brodersen CR, Lee EF, Choat B, Jansen S, Phillips RJ, Shackel KA, McElrone AJ, Matthews MA. 2011. Automated analysis of three-dimensional xylem networks using high-resolution computed tomography. *New Phytologist* **191**: 1168–1179.

Brodersen CR, McElrone AJ, Choat B, Lee EF, Shackel KA, Matthews MA. 2013. *In vivo* visualizations of drought-induced embolism spread in *Vitis vinifera*. *Plant Physiology* **161**: 1820–1829.

Brodersen CR, McElrone AJ, Choat B, Matthews MA, Shackel KA. 2010. The dynamics of embolism repair in xylem: *in vivo* visualizations using high-resolution computed tomography. *Plant Physiology* **154**: 1088–1095.

Brodribb TJ, Cochard H. 2009. Hydraulic failure defines the recovery and point of death in water-stressed conifers. *Plant Physiology* **149**: 575–584.

Butterfield B, Philipson W, Meylan B, Ohtani J. 1984. Comparative morphology of the vessel elements in the woods of *Pseudopanax* C. Koch (Araliaceae). *New Zealand Journal of Botany* **22**: 509–514.

Canny M. 1997. Vessel contents during transpiration-embolisms and refilling. *American Journal of Botany* **84**: 1223.

Carlquist S. 2001. *Comparative wood anatomy: systematic, ecological, and evolutionary aspects of dicotyledon wood*. Berlin, Germany: Springer Science & Business Media.

Charrier G, Torres-Ruiz JM, Badel E, Burlett R, Choat B, Cochard H, Delmas CE, Domec J-C, Jansen S, King A. 2016. Evidence for hydraulic vulnerability segmentation and lack of xylem refilling under tension. *Plant Physiology* **172**: 1657–1668.

Choat B, Brodersen CR, McElrone AJ. 2015. Synchrotron X-ray microtomography of xylem embolism in Sequoia sempervirens saplings during cycles of drought and recovery. *New Phytologist* **205**: 1095–1105.

Choat B, Jansen S, Brodribb TJ, Cochard H, Delzon S, Bhaskar R, Bucci SJ, Feild TS, Gleason SM, Hacke UG. 2012. Global convergence in the vulnerability of forests to drought. *Nature* **491**: 752–755.

Christman MA, Sperry JS. 2010. Single-vessel flow measurements indicate scalariform perforation plates confer higher flow resistance than previously estimated. *Plant, Cell & Environment* **33**: 431–443.

Clearwater MJ, Goldstein G. 2005. Embolism repair and long distance water transport. In: Holbrook NM, Zwieneicki MA, eds. *Vascular transport in plants*. Burlington, MA, USA: Elsevier Academic Press, 375–399.

Cochard H, Delzon S, Badel E. 2015. X-ray microtomography (micro-CT): a reference technology for high-resolution quantification of xylem embolism in trees. *Plant, Cell & Environment* **38**: 201–206.

Cochard H, Hölttä T, Herbette S, Delzon S, Mencuccini M. 2009. New insights into the mechanisms of water-stress-induced cavitation in conifers. *Plant Physiology* **151**: 949–954.

Davis SD, Sperry JS, Hacke UG. 1999. The relationship between xylem conduit diameter and cavitation caused by freezing. *American Journal of Botany* **86**: 1367–1372.

Ewers FW. 1985. Xylem structure and water conduction in conifer trees, dicot trees, and lianas. *IAWA Journal* **6**: 309–317.

Frost FH. 1930. Specialization in secondary xylem of dicotyledons. II. Evolution of end wall of vessel segment. *Botanical Gazette* **90**: 198–212.

Hochberg U, Windt CW, Ponomarenko A, Zhang Y-J, Gersony J, Rockwell FE, Holbrook NM. 2017. Stomatal closure, basal leaf embolism and shedding protect the hydraulic integrity of grape stems. *Plant Physiology* **174**: 764–775.

Holbrook NM, Ahrens ET, Burns MJ, Zwieniecki MA. 2001. *In vivo* observation of cavitation and embolism repair using magnetic resonance imaging. *Plant Physiology* **126**: 27–31.

Holbrook NM, Zwieniecki MA. 1999. Embolism repair and xylem tension: do we need a miracle? *Plant Physiology* **120**: 7–10.

Knipfer T, Brodersen CR, Zedan A, Kluepfel DA, McElrone AJ. 2015a. Patterns of drought-induced embolism formation and spread in living walnut saplings visualized using X-ray microtomography. *Tree Physiology* **35**: 744–755.

Knipfer T, Cuneo IF, Brodersen CR, McElrone AJ. 2016. *In situ* visualization of the dynamics in xylem embolism formation and removal in the absence of root pressure: a study on excised grapevine stems. *Plant Physiology* **171**: 1024–1036.

Knipfer T, Eustis A, Brodersen C, Walker AM, McElrone AJ. 2015b. Grapevine species from varied native habitats exhibit differences in embolism formation/repair associated with leaf gas exchange and root pressure. *Plant, Cell & Environment* **38**: 1503–1513.

Kohonen MM, Helland Å. 2009. On the function of wall sculpturing in xylem conduits. *Journal of Bionic Engineering* **6**: 324–329.

Konrad W, Roth-Nebelsick A. 2005. The significance of pit shape for hydraulic isolation of embolized conduits of vascular plants during novel refilling. *Journal of Biological Physics* **31**: 57–71.

Lee S-J, Kim Y. 2008. *In vivo* visualization of the water-refilling process in xylem vessels using X-ray micro-imaging. *Annals of Botany* **101**: 595–602.

Lens F, Vos RA, Charrier G, van der Niet T, Merckx V, Baas P, Aguirre Gutierrez J, Jacobs B, Chacon Dória L, Smets E. 2016. Scalariform-to-simple transition in vessel perforation plates triggered by differences in climate during the evolution of Adoxaceae. *Annals of Botany* **118**: 1043–1056.

McCully M, Canny M, Baker A, Miller C. 2014. Some properties of the walls of metaxylem vessels of maize roots, including tests of the wettability of their lumenal wall surfaces. *Annals of Botany* **113**: 977–989.

Meylan B, Butterfield B. 1975. Occurrence of simple, multiple, and combination perforation plates in the vessels of New Zealand woods. *New Zealand Journal of Botany* **13**: 1–18.

Oertli J. 1971. Stability of water under tension in the xylem. *Zeitschrift fur Pflanzenphysiologie* **65**: 195–209.

Oskolski AA, Jansen S. 2009. Distribution of scalariform and simple perforation plates within the vessel network in secondary xylem of Araliaceae and its implications for wood evolution. *Plant Systematics and Evolution* **278**: 43–51.

R Core Team 2013. *R: A language and environment for statistical computing*. Vienna, Austria: R Foundation for Statistical Computing. URL http://www.R-project.org/ [accessed 9 February 2017].

Rolland V, Dana MB, Lenné T, Bryant G, Chen H, Wolfe J, Holbrook NM, Daniel ES, Marilyn CB. 2015. Easy come, easy go: capillary forces enable rapid refilling of embolized primary xylem vessels. *Plant Physiology* **168**: 1636–1647.

Ryu J, Hwang BG, Kim YX, Lee SJ. 2016. Direct observation of local xylem embolisms induced by soil drying in intact *Zea mays* leaves. *Journal of Experimental Botany* **67**: 2617–2626.

Schenk HJ, Espino S, Romo DM, Nima N, Do AY, Michaud JM, Papahadjopoulos-Sternberg B, Yang J, Zuo YY, Steppe K. 2017. Xylem surfactants introduce a new element to the cohesion-tension theory. *Plant Physiology* **173**: 1177–1196.

Schenk HJ, Steppe K, Jansen S. 2015. Nanobubbles: a new paradigm for air-seeding in xylem. *Trends in Plant Science* **20**: 199–205.

Scholander P, Love WE, Kanwisher JW. 1955. The rise of sap in tall grapevines. *Plant Physiology* **30**: 93.

Sperry JS. 1985. Xylem embolism in the palm *Rhapis excelsa*. *IAWA Journal* **6**: 283–292.

Sperry JS. 2003. Evolution of water transport and xylem structure. *International Journal of Plant Sciences* **164**(S3): S115–S127.

Sperry JS, Holbrook NM, Zimmermann MH, Tyree MT. 1987. Spring filling of xylem vessels in wild grapevine. *Plant Physiology* **83**: 414–417.

Tyree MT, Salleo S, Nardini A, Gullo MAL, Mosca R. 1999. Refilling of embolized vessels in young stems of laurel. Do we need a new paradigm? *Plant Physiology* **120**: 11–22.

Tyree MT, Zimmermann MH. 2002. *Xylem structure and the ascent of sap*. Berlin, Germany: Springer Science & Business Media.

Urli M, Porté AJ, Cochard H, Guengant Y, Burlett R, Delzon S. 2013. Xylem embolism threshold for catastrophic hydraulic failure in angiosperm trees. *Tree Physiology* **33**: 672–683.

Wegner LH. 2013. Root pressure and beyond: energetically uphill water transport into xylem vessels? *Journal of Experimental Botany* **65**: 381–393.

Yang S, Tyree M. 1992. A theoretical model of hydraulic conductivity recovery from embolism with comparison to experimental data on *Acer saccharum*. *Plant, Cell & Environment* **15**: 633–643.

Supporting Information

Additional Supporting Information may be found online in the Supporting Information tab for this article:

Fig. S1 Recovery of stem-equilibrated leaf water potential for three *V. vinifera* plants after soil saturation.

Please note: Wiley Blackwell are not responsible for the content or functionality of any Supporting Information supplied by the authors. Any queries (other than missing material) should be directed to the *New Phytologist* Central Office.